Article

Alkaline Reduced Water Attenuates Oxidative Stress-Induced Mitochondrial Dysfunction and Innate Immune Response Triggered by Intestinal Epithelial Dysfunction

Jayson M. Antonio [1,2], Ailyn Fadriquela [3], Yun Ju Jeong [4], Cheol-Su Kim [4] and Soo-Ki Kim [1,*]

1   Department of Microbiology, Wonju College of Medicine, Yonsei University, Wonju 26426, Korea; jayson.antonio@dlsu.edu.ph
2   Department of Global Medical Science, Wonju College of Medicine, Yonsei University, Wonju 26426, Korea
3   Department of Laboratory Medicine, Wonju College of Medicine, Yonsei University, Wonju 26426, Korea; ailyn@yonsei.ac.kr
4   Department of Environmental Medical Biology, Wonju College of Medicine, Yonsei University, Wonju 26426, Korea; joj2337@naver.com (Y.J.J.); cs-kim@yonsei.ac.kr (C.-S.K.)
*   Correspondence: kim6@yonsei.ac.kr; Tel.: +82-33741-0331

Abstract: Redox imbalance in intestinal epithelial cells is critical in the early phases of intestinal injury. Dysfunction of the intestinal barrier can result in immunological imbalance and inflammation, thus leading to intestinal syndromes and associated illnesses. Several antioxidants have been discovered to be beneficial in resolving intestinal barrier dysfunction. Of these antioxidants, the effects of alkaline reduced water (ARW) in oxidative stress of intestinal epithelial cells and its immunokine modulation in vitro is unknown. In this study, we utilized ARW-enriched media to investigate its cytoprotective effect against H_2O_2-induced oxidative stress in DLD1 cells. We found that ARW rescued DLD1 from oxidative stress by diluting the influence of H_2O_2 on oxidative stress-activated MAPK signaling and mitochondrial dysfunction. Further, intestinal oxidative stress significantly affects immunokine profiles of Raw 264.7 cells (IL-6, IL-10, MCP, TNF-a, RANTES), which can be reversed by ARW. Collectively, ARW shields intestinal epithelial cells from oxidative stress, reducing the immunological mayhem caused by barrier failure.

Keywords: alkaline reduced water; oxidative stress; cytokines; MAPK; mitochondrial dysfunction

1. Introduction

The intestinal barrier is an intricate structure comprising of networks of cells and extracellular matrixes that highly regulate the selectively permeable function of the gut barrier [1]. It warrants nutrient absorption while perpetually impeding the transport of hazardous antigens and bacteria from the gut lumen [2]. As the intestinal barrier is continually exposed to innocuous and perilous stimuli, it is regarded as a key regulator of reactive oxygen species (ROS) [3]. Of the intestinal components, the robustness of intestinal epithelial cells is critical for the intestinal barrier [4]. The intestinal epithelium generates a plethora of defense mechanisms to preserve proper physiological function in the face of oxidative stress [5]. Importantly, excessive alterations to intestinal epithelial homeostasis may exacerbate intestine porousness to noxae, thereby hastening the progression of intestinal and nonintestinal disorders [6].

Endogenous ROS are known to be generated regularly in cells as a result of a variety of biological activities and metabolic processes [7]. Most of the ROS are produced by the mitochondria. However, because of their unstable, active, and pleiotropic properties, these molecules intermingle with a wide array of cellular components, including proteins, lipids, and DNA, as well as different cellular organelles, and influence various signaling pathways [8,9]. Excessive ROS can cause oxidative stress leading to overstimulation of mitogen-activated protein kinase (MAPK) signaling, mitochondrial malfunction, and

apoptosis [9,10]. Thus, ROS can generate both constructive and destructive effects on the cell and should be tightly monitored and controlled by various antioxidant systems to prevent oxidative stress [11].

In the context of ROS and gut illnesses, oxidative stress can induce intestinal epithelial cell malfunction, wreaking havoc on the intestinal barrier and culminating in a variety of intestinal, cardiovascular, and neurological problems, as well as a shorter life expectancy [11]. Consequently, exogenous antioxidants in the form of dietary nutrients such as vitamins, minerals, amino acids, peptides, and fatty acids were evaluated for their potential to maintain a vigorous intestinal barrier [12–17]. In addition, polyphenols, isoflavones, flavonoids, glycosides, and polysaccharides are some of the bioactive natural compounds that also protect intestinal cells from oxidative damage [18,19]. Further, these nutraceuticals act as probiotics, influencing the diversity and composition of gut flora, which can directly and indirectly maintain the gut barrier [19].

Considering the aforementioned facts, alkaline reduced water (ARW) can be a low-cost and noncaloric therapeutic intervention for intestinal illnesses due to its strong antioxidant potential, which is enhanced by its high H_2 content and low oxidation reduction potential (ORP) [20]. ARW is widely known to exert anti-inflammatory and anticancer effects, among its other bioactive properties [21–23]. Likewise, clinical trials have indicated that ARW therapy may prevent gastrointestinal disorders including gastritis and irritable bowel syndrome [24–26]. However, the mechanism through which ARW protects intestinal epithelial cells from oxidative stress remains an open question. Thus, this study was conducted using DLD1 and RAW 264.7 cell lines to investigate how ARW maintains the intestinal barrier and immunological function under oxidative stress. Herein, we report that ARW regulates MAPK signaling and maintains mitochondrial function in cultured cells which supports immunological balance during oxidative stress.

2. Materials and Methods

2.1. Media Preparation and Cell Cultures

Sodium bicarbonate (2 g) was added to Gibco™ RPMI 1640 Medium, powder (CAT 31800022) and dissolved with 100 mL of water. The resulting RPMI stock was labeled as $10\times$ stock. To prepare the control media and ARW media, the $10\times$ stock was reconstituted with distilled water (dH_2O group), alkaline water pH 8.5 (pH 8.5 group), and alkaline water pH 10 (pH 10 group) (Hanumul Co., Ltd., Goyang, Korea) to make $1\times$ RPMI media, and was filtered and sterilized. The DLD-1 human colon cancer cell line (American Type Culture Collection, ATCC, CCL-221™, Manassas, VA, USA) and RAW 264.7 macrophage cell line (American Type Cell Culture Collection, Manassas, VA, USA) were cultured in control media (dH_2O) supplemented with 5% FBS, 100 U/mL penicillin, and 100 µg/mL streptomycin, at 37 °C, in a humidified atmosphere containing 5% CO_2. To identify the ideal dose and time for H_2O_2 stimulation, the culture medium was replaced by dH_2O, pH 8 and pH 10 media and DLD-1 cells were treated with 2-fold dilution series of H_2O_2 (0–2000 µM) for 24 h and cell viability was identified using a crystal violet cell cytotoxicity assay kit (BioVision, Milpitas, CA, USA) following the manufacturer's protocol.

2.2. Scratch Wound Healing Assay

Cells were seeded in 35 mm dish using dH_2O media until confluent. Scratch wound healing assay was performed wherein cells were mechanically wounded. The culture medium was replaced by control and experimental media and cell were treated with 330 µM of H_2O_2 for 12 h. The treatment was withdrawn and replaced with control and experimental media. Cell migration was observed at 0, 48, and 60 h. Cells were stained with crystal violet (BioVision, Milpitas, CA, USA) for better visualization.

2.3. Western Blot Analysis

Expressions of p-ERK, p-p38, pDRP1, and OPA-1 were measured using Western blotting. The normalized protein concentration of cell lysate was equally loaded and

separated by electrophoresis on sodium dodecyl sulfate-polyacrylamide gels and was transferred to a polyvinylidene difluoride membrane. The membrane was blocked in 5% skim milk for 1 h. Then, the membranes were incubated with primary antibodies overnight at 4 °C. The membrane was then incubated with horseradish peroxidase (HRP)-conjugated secondary antibodies for 1 h at room temperature. Chemiluminescent detection was performed using the Chemiluminescence Western blot Detection System (BioSpectrum® 600 Imaging System, Upland, CA, USA). Primary antibodies used were the following: β-actin, p-p38, p-ERK1/2, ERK1/2, pDRP1 (S616), DRP1, OPA1 (dilution: 1:2000, Cell Signaling Technology, Danvers, MA, USA). Immunoreactive bands were quantified using Image Lab 6.0 (Bio-Rad, Hercules, CA, USA).

2.4. Catalase Assay

A catalase assay was performed according to the manufacturer's protocol (BioVision, Milpitas, CA, USA). In brief, standards were prepared to generate 0, 2, 4, 6, 8, 10 nmol/well of H_2O_2 standard. Cell lysate samples and standards were added to a 96-well plate. Then, 1 mM of H_2O_2 was added to the samples and the plate was incubated at 25 °C for 30 min before adding the stop solution. A reaction mix (50 µL) was then prepared and added to each sample and standard. The plate was incubated at 25 °C for 10 min and was measured at OD 570 nm. Catalase activity was calculated according to the decomposed H_2O_2 amount.

2.5. Multiplex Assay

Immunokine profiling was performed using the Milliplex® MAP Human Immuno-Oncology Checkpoint Protein Magnetic Bead Panel 96-well plate assay (Millipore Corporation, Billerica, MA, USA) as a luminex-based multiplex technology. Interleukin (IL)-6, IL-10, tumor necrosis factor (TNF)-α, monocyte chemoattractant protein (MCP)-1, regulated on activation, normal T expressed and secreted (RANTES), granulocyte colony-stimulating factor (G-CSF), keratinocyte chemoattractant (KC), vascular endothelial growth factor (VEGF), and interferon gamma-induced protein (IP) 10 were measured using a multiplex immunoassay following the manufacturer's protocol. In brief, each standard concentration was resuspended in standard diluents, and serial dilutions of the standard were prepared. The bead mixture was added to the standard and cell lysate. The plate was incubated overnight (18 h) at 4 °C and was proceeded by a washing step. Detection antibody was added, and the plate was incubated at room temperature for 1 h. Streptavidin-phycoerythrin mix was added and the plate was incubated at room temperature for 30 min. After the washing step, an assay buffer was added, and the plate was analyzed using the Luminex 200 Bio-Plex instrument.

2.6. TMRE Mitochondrial Membrane Potential Measurement

DLD1 (3×10^4) were suspended in 500 µL of complete medium or ARW medium before being seeded on to 12 mm L-poly-lysine coated coverslips embedded in a 4-well plate and treated with H_2O_2 (330 µM, 24 h). To measure mitochondrial membrane potential, cells were treated for 20 m with 100 nM TMRE (Sigma-Aldrich, Burlington, MA, USA) dissolved in Ca^{2+} KRBB, washed 3 times with KRBB, then perfused with Ca^{2+} KRB buffer in the presence of 100 nM TMRE. The chamber was mounted on the IX-73 inverted microscope platform (Olympus Corporation, Tokyo, Japan) with a camera attachment (Prime-BSI CMOS camera, Teledyne Photometrics, Tucson, AZ, USA) and an illumination (CoolLED, Andover, UK). The fluorophore was stimulated alternatively at 530 nm and 45 nm full width at half-maximum transmission. MetaFluor 6.1 was used to acquire images (Molecular Devices, San Jose, CA, USA). Background was removed, and changes were computed. At the end of each experiment, 2 M FCCP dissolved in 1.5 mM Ca^{2+} KRBB was added to achieve a maximum ratio for comparison between the control and ARW groups.

2.7. Mitochondrial Morphology

DLD1 (3×10^4) cells were seeded on to 12 mm L-poly-lysine coated coverslips embedded in a 4-well plate using dH_2O media and incubated for 24 h. The media was discarded

and replaced with control and experimental media and cells were treated with H_2O_2 (330 μM, 24 h). Cells were washed with PBS, and incubated with Mitotracker (Molecular Probes), at final concentrations of 150 nM the cells were added into fresh medium. Mito-Tracker Green Fluorescence was then visualized using a fluorescent microscope (Olympus BX51 Fluorescence Microscope, Olympus Corporation, Tokyo, Japan). For quantification, images from 40 cells per condition were collected and then blinded these images. Three researchers then scored the cells for containing primarily fragmented, tubular, or elongated mitochondria.

2.8. Data Management and Statistical Analysis

Heatmapping was performed using the Morpheus site (broadinstitute.org). First, data was normalized according to the Z score. Z score was calculated by the following formula: Z score = (real value-mean value)/standard deviation. The data file was uploaded to the site and data presentation of the heatmap was set and modified according to the desired presentation. Data standards were taken with mean value $\pm$ standard error mean (SEM). All data in each marker were normalized and fold change was computed according to normal control and was analyzed and compared by one-way analysis of variance (ANOVA), followed by subsequent multiple comparison test (Tukey post hoc test) with GraphPad Prism 8.0 software package (Graph-Pad, La Jolla, CA, USA). Differences were considered statistically significant at $p < 0.05$.

3. Results

3.1. ARW Promotes Cytoprotective and Promigratory Effecs in DLD1 Cells under Oxidative Stress Condition

To test the cytoprotective and promigratory effect of ARW in intestinal epithelial cells, we prepared three sets of cell culture media (dH$_2$O, pH 8.5 and pH 10). As shown in the table (Figure 1a), utilizing ARW in culture media preparation had no effect on the pH and osmolarity of the RPMI media. As expected, the concentration of H_2 in ARW-enriched medium is substantially higher than in normal media (dH$_2$O). However, the concentration of H_2 in the ARW-enriched medium returns to normal after 15 min (Figure 1b).

This prompted us to use a freshly prepared ARW medium in all our experiments. To investigate H_2O_2-induced cell death in the intestinal epithelium, we utilized DLD1 cell lines which demonstrated enterocyte-like epithelial cell features. We determine the IC$_{50}$ of H_2O_2 using a 2-fold dilution series in DLD1 colon cancer cells after 24 h of exposure. Figure 1c shows the concentration-dependent cytotoxicity of H_2O_2. In dH$_2$O, the DLD1 exposed to H_2O_2 exhibited a drastic increase in cell mortality as early as 326.1 ± 4.54 μM. On the contrary, the cells maintained in the media prepared using ARW pH 8.5 and pH 10 displayed a significant increase in cell viability under H_2O_2 treatment with IC$_{50}$ values of 347 ± 4.22 μM ($p < 0.01$) and 428.8 ± 4.27 μM ($p < 0.0001$), respectively (Figure 1d). This result indicated that ARW had a cytoprotective effect against H_2O_2-induced cell apoptosis. We further confirmed the effects of ARW on the restoration of DLD1 cells by scratch-wound healing assay (Figure 1e,f). Confluent DLD1 cells were mechanically wounded and treated with 330 μM of H_2O_2 for 12 h. The treatment was withdrawn and replaced by normal or ARW-enriched media. As shown in Figure 1e,f, the ARW pH 8.5 and pH 10 significantly enhanced cell migration, recovering $63.97 \pm 6.81\%$ ($p < 0.01$) and $86.66 \pm 8.44\%$ ($p < 0.001$) of wounded area at 60 h, respectively, compared to $54.53 \pm 6.01\%$ in the dH$_2$O group (Figure 1e,f). These results suggested that ARW ameliorates H_2O_2-induced deferment in wound repair.
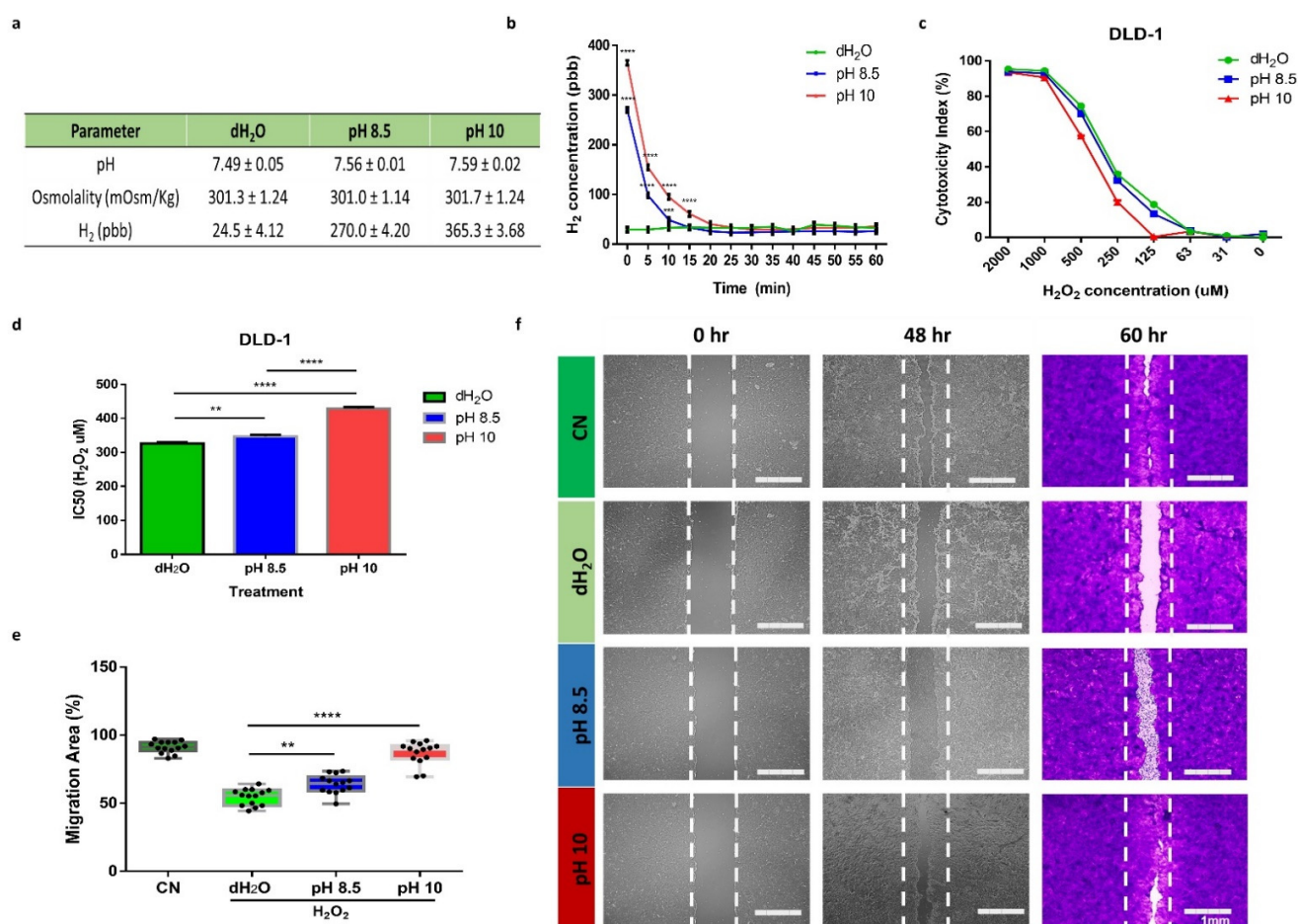
Figure 1. Cytoprotective and promigratory effects of ARW in H_2O_2-induced DLD1 cells: (**a**) Characteristics of the 3 cell culture media. (**b**) H_2 concentration of culture media. (**c**,**d**) Cytotoxicity index plot and IC_{50} of DLD1 cells after 24 h exposure to H_2O_2. (**e**) Quantitative results of DLD1 migration. (**f**) Time-lapse images of a representative scratch assay from each group are plotted at 0, 48, and 60 h. Values are stated as mean $\pm$ SD. The significant difference was analyzed with one-way ANOVA and Tukey's test, ** $p < 0.01$, *** $p < 0.001$, **** $p < 0.0001$. Abbreviation: control (CN), normal media (dH$_2$O), ARW pH 8.5 (pH 8.5), ARW pH 10 (pH 10).

3.2. ARW Attenuated Overactivation of ROS-Regulated Signal Pathways

Several studies showed that H_2O_2 induces activation of MAPK signaling pathway. ERK1/2 and p38 kinases are sensitive to oxidative stress and can promote both prosurvival and proapoptotic effects. We examined the phosphorylation of ERK1/2 in DLD1 cells exposed to 330 μM H_2O_2 for 24 h. We detected appreciable ERK1/2 activation in dH$_2$O ($p < 0.01$) group compared to CN, pH 8.5 and pH 10 groups (Figure 2a). We also showed augmented phosphorylation or activation of p38 in the dH$_2$O group ($p < 0.001$) compared to CN and ARW groups. Interestingly, both pH 8.5 and pH 10 groups dramatically attenuated H_2O_2-induced p38 activation ($p < 0.001$), even lower than the CN group (Figure 2b). Further, we examined H_2O_2-induced oxidative stress in DLD1 cells by measuring the activity of endogenous antioxidant catalase. The treatment of H_2O_2 significantly stimulated catalase activity in the dH$_2$O group ($p < 0.0001$) compared to the CN and ARW groups (Figure 2c). These results indicate that ARW counteracts H_2O_2-induced intestinal epithelial cell injury by mitigating the activation of signal transduction pathways during oxidative stress.
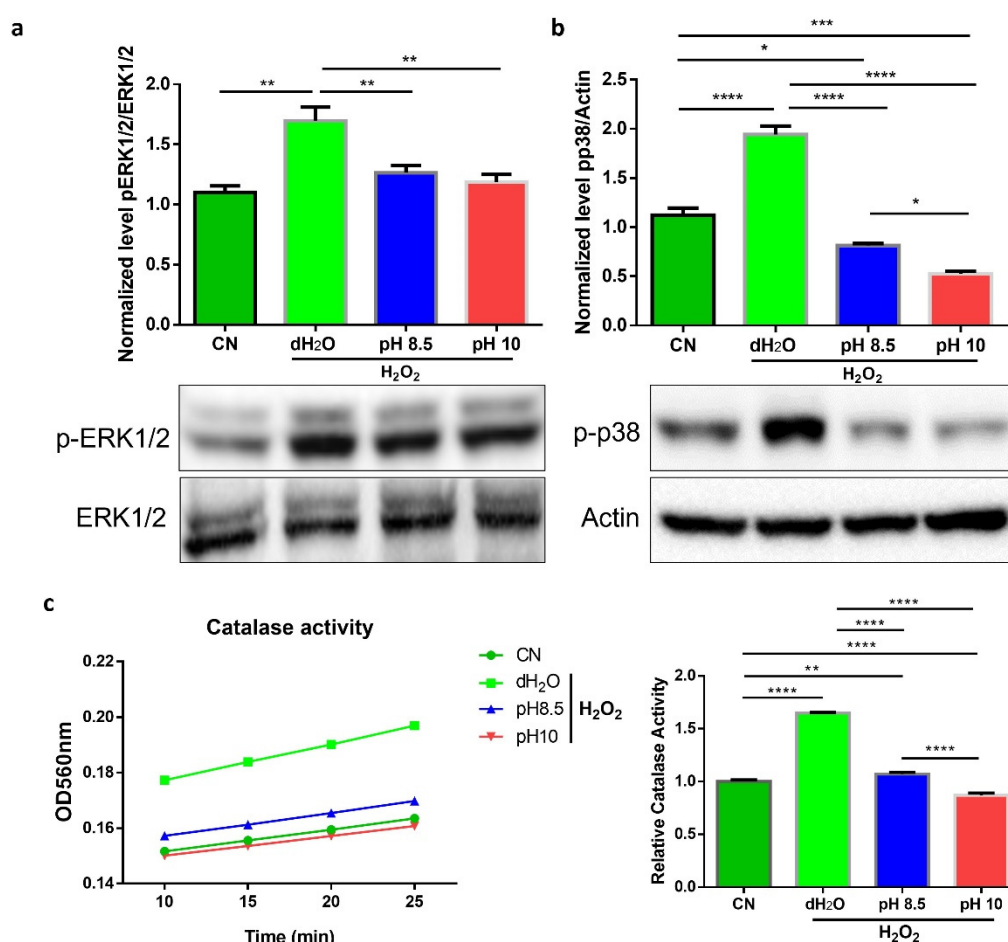
Figure 2. ARW recovered MAPK and catalase activity of H_2O_2-induced DLD1 cells: (**a**,**b**) Western blot analysis and quantification of the phosphorylation of ERK1/2 and p38. (**c**) Estimation of catalase enzyme activity in cell lysate of DLD1 exposed to H_2O_2 for 24 h. Values are stated as mean ± SD, *n* = 3. The significant difference was analyzed with one-way ANOVA and Tukey's test, * $p < 0.05$, ** $p < 0.01$, *** $p < 0.001$, **** $p < 0.0001$. Abbreviation: control (CN), normal media (dH$_2$O), ARW pH 8.5 (pH 8.5), ARW pH 10 (pH 10), optical density (OD).

3.3. ARW Protects Mitochondria from H_2O_2-Induced Oxidative Damage in DLD1 Cells

Mitochondria are cell organelles that are susceptible to oxidative damage. H_2O_2 is a known pathogenic factor in mitochondrial dysfunction. To assess the protective effects of ARW against H_2O_2-induced mitochondrial damage in DLD1 cells, we measured the mitochondrial membrane potential using TMRE (Figure 3a). The treatment of H_2O_2 led to a significant decrease in the mitochondrial membrane potential in dH$_2$O and ARW groups ($p < 0.0001$) compared to the CN group. However, the ARW treatments pH 8.5 and pH 10 partially rescued mitochondrial membrane potential to control levels. Since mitochondrial membrane potential is critical for maintaining mitochondrial bioenergetics and dynamics, we investigated the effects of ARW in mitochondrial morphology of DLD1 cells under disturbed redox state. We found that H_2O_2 treatment significantly increased phosphorylation of DRP1 at the serine 616 (pDRP1 S616) site, which promotes mitochondrial fragmentation (Figure 3b). Interestingly, ARW pH 8.5 and pH 10 dramatically abated pDRP1 levels compared to the dH$_2$O group. We also assessed the level of long IMM-bound OPA1 (L-OPA1) and short-soluble OPA1 (S-OPA1) forms that modulate mitochondrial fusion. Surprisingly, the oxidative stress strikingly decreased the ratio of L-OPA1 to S-OPA1, but the preeminent decline was observed from the dH$_2$O group ($p < 0.0001$). These results suggested that ARW ameliorates the excessive increase in mitochondrial fragmentation in oxidative stress conditions and alerted redox states. Further, we visualized structural changes in mitochondria after H_2O_2 treatment by fluorescent light microscopy. We con-

firmed that most mitochondria transformed from the classic tubular shape into fragmented structures during oxidative stress in DLD1 cells (Figure 3c). Remarkably, the ARW treatment rescues DLD1 cells from H_2O_2-induced mitochondrial fragmentation, suggesting the mitochondrial-restoring function of ARW.
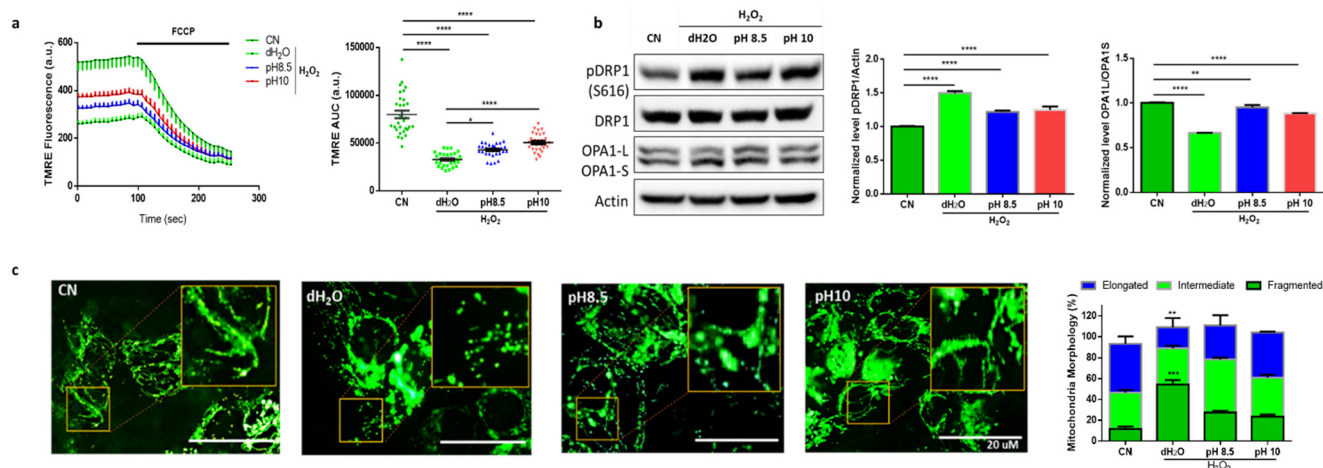

Figure 3. ARW restrained mitochondrial dysfunction in H_2O_2-induced DLD1 cells: (**a**) Effects of ARW on the mitochondrial membrane potential of H_2O_2-induced DLD1. (**b**) Western blot analysis and quantification of the phosphorylation of DRP1, and OPA1. (**c**) Representative images and mitochondrial quantification (n = 50 cells/ treatment) of DLD1 in CN, dH_2O, pH 8 and pH 10. Data represent mean $\pm$ SD of two independent experiments, The significant difference was analyzed with one-way ANOVA, * $p < 0.05$, ** $p < 0.01$, *** $p < 0.001$, **** $p < 0.0001$. Abbreviation: control (CN), normal media (dH_2O), ARW pH 8.5 (pH 8.5), ARW pH 10 (pH 10), arbitrary units (a.u.), tetramethylrhodamine, ethyl ester (TMRE), area under curve (AUC).

3.4. ARW Counteracts Activation of Innate Immune Response Triggered by Intestinal Dysfunction

We utilized DLD1 as an in vitro model of the intestinal barrier and investigated how oxidative stress in intestinal epithelial cells fine-tunes the innate immune response. In the diagram (Figure 4a), the DLD1 cells were exposed to H_2O_2 treatment for 24 h. The culture supernatant from DLD1 was added to RAW 264.7 cells macrophage (20% of DLD1 culture medium v/v), and the cells were maintained for 24 h. We then performed cytokine/chemokine profiling on macrophage cell lysate using Bio-Plex (Bio-Rad). Captivatingly, compared with the untreated control (unCN) group, the DLD1 culture supernatant (CN group) did not change the macrophage cytokine/chemokine profile (Figure 4b,c). However, culture supernatant from DLD1 exposed to H_2O_2 caused a plethora of changes in immunokine profiles of the macrophage. The levels of IL-6 ($p < 0.01$), IL-10 ($p < 0.01$), TNF-α ($p < 0.01$), MCP-1 ($p < 0.05$) and RANTES ($p < 0.05$) were increased substantially in dH_2O group compared to ARW and CN groups. No significant differences were observed in the levels of G-CSF, KC, VGEF, and IP-10 among the groups (Figure 4c). These data show that ARW would neutralize the effect of oxidative stress in the intestinal epithelial cell-derived innate immune response.
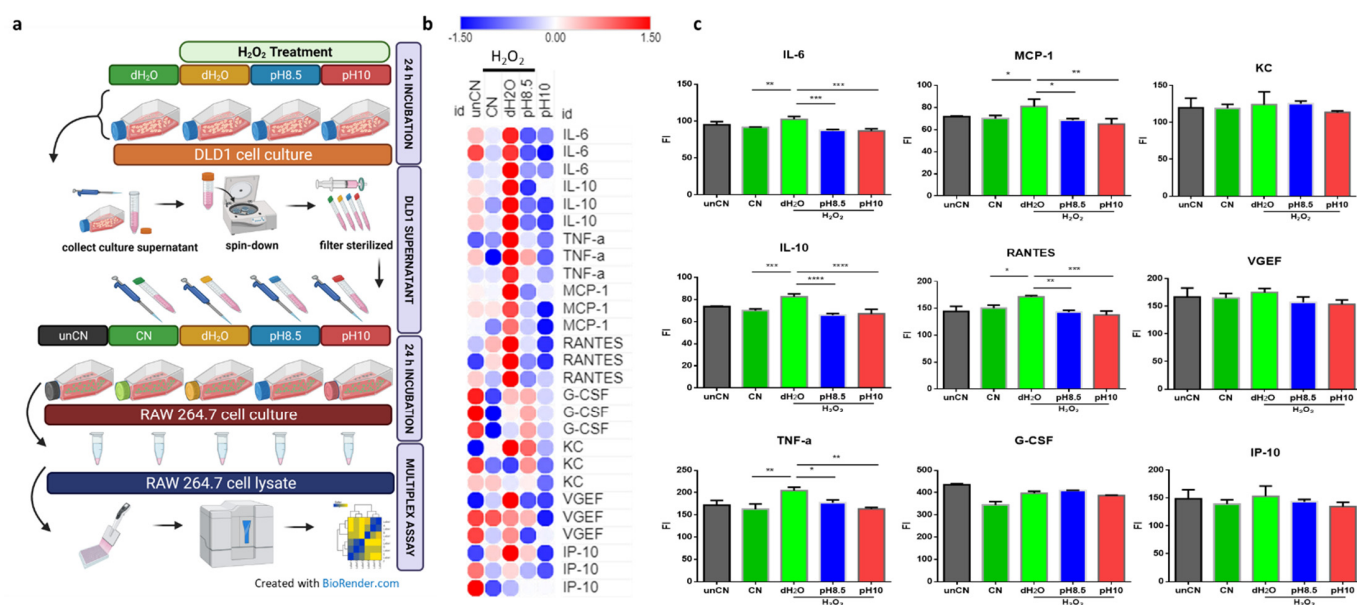
Figure 4. Activation of innate immune response triggered by intestinal dysfunction is suppressed by ARW. (**a**) Schematic diagram depicting DLD1 cell culture supernatant preparation. Filter sterilized cell culture supernatants from DLD1 were treated to RAW 264.7 macrophage. Cell lysates of macrophage were analyzed using multiplex assay. (**b**) Heat map showing changes in the levels of cytokines/chemokines in RAW 264.7 cell lysate. Data were normalized (z-score values). (**c**) Levels of chemokines/cytokines in RAW 264.7 lysate (fluorescent intensity). Data represent mean ± SD of two independent experiments, the significant difference was analyzed with one-way ANOVA ($n = 3$), * $p < 0.05$, ** $p < 0.01$, *** $p < 0.001$, **** $p < 0.0001$. Abbreviation: untreated control (unCN), control (CN), normal media (dH$_2$O), ARW pH 8.5 (pH 8.5), ARW pH 10 (pH 10), fluorescence intensity (FI), interleukin 6 (IL-6), interleukin 10 (IL-10), tumor necrosis factor -α (TNF-α), monocyte chemoattractant protein 1 (MCP-1), regulated on activation, normal T expressed and secreted (RANTES), granulocyte colony-stimulating factor (G-CSF), keratinocyte chemoattractant (KC), vascular endothelial growth factor (VEGF), and interferon gamma-induced protein 10 (IP-10).

4. Discussion

ARW has various biological potentials, including anticancer and anti-inflammation properties. However, the effect of ARW on intestinal barrier dysfunction and immunological modulation has remained unknown. Thus, we evaluated the protective effects of ARW in the intestinal barrier by examining cell viability, MAPK signaling, and mitochondrial dynamics. Further, we also investigated immunokine expression in vitro to determine how a disturbed intestinal barrier affects immunological cadence. In the present study, we provide the first evidence that ARW could exert cytoprotective effects on intestinal epithelial cells after oxidative stress. Using DLD1 as an intestinal barrier model, we demonstrated that ARW-enriched medium could effectively rescue the cells and promote wound healing in DLD1 following oxidative stress. The antioxidative stress action of ARW was further confirmed by MAPK signaling and mitochondrial dynamics analyses, which revealed that ARW maintains pERK1/2 and pp38 at stable levels and prevents excessive mitochondrial fission and mitochondrial membrane depolarization. Moreover, ARW inhibits the inflammatory immunokine activation in macrophages produced by oxidative stress in intestinal epithelial cells.

This study clearly demonstrates through four ways that ARW attenuates oxidative stress in the intestinal barrier. First of all, we showed that ARW protects intestinal epithelial cells from H$_2$O$_2$-induced apoptosis using the colorectal adenocarcinoma cell line DLD1. DLD1 has been used as a model for the intestinal barrier because it retains enterocyte barrier properties such as the terminal bar and intercellular cohesion [27]. In view of this, we determined the growth rate and cell viability of DLD1 in both normal and ARW-enriched media for 5 days (data not shown). We found no significant differences in the growth rate and cell viability of DLD1 in both ARW-enriched media and normal media.

We induced oxidative stress in DLD1 using H_2O_2, which resulted in a dose-dependent cytotoxicity response. As expected, both the pH 8.5 and pH 10 ARW-enriched media rescued the cell from the cytotoxic effect of H_2O_2. Several studies have shown that ARW has cytoprotective effects against oxidative stress in various cell types [21,28], which supports our findings. We further found that ARW-enriched medium promoted promigratory action and wound healing in H_2O_2-induced DLD1. These results might be related to the antioxidant property of ARW. Antioxidant treatment prior to H_2O_2 exposure greatly improved the wound healing ability of examined cells [29,30]. On this account, we assumed that the antioxidant properties of ARW were attributable to its supramaximal H_2 level; however, the concentration of H_2 in ARW culture media returned to normal levels after 20 min, contradicting our hypothesis. This is important because at normal H_2 levels, the ARW still elicits cytoprotective activity against oxidative stress. Similar to our study, the degassed, electrolyzed, reduced water exhibited substantial ROS-scavenging activity [31]. These data suggest that the ARW produced by a Hanumul Co., LTD water purifier has a nongaseous antioxidant factor.

Next, we found that ARW reduces H_2O_2-induced oxidative damage in DLD1 by assessing the MAPK signaling and catalase activity. Though this signaling might be proapoptotic or antiapoptotic, we discovered pERK1/2 and pp38 were stimulated in DLD1 treated with H_2O_2. The role of MAPK signaling during oxidative stress is still controversial. Some studies have demonstrated that MAPK activation is necessary to rescue cells from oxidative damage and that pharmacological inhibition of MAPK signaling enhances cytotoxicity in H_2O_2-induced cells [32,33]. Other studies have shown opposite results, that blocking MAPK signaling aids cell survival in the state of redox imbalance [34,35]. However, it is widely acknowledged that antioxidants protect cells against oxidative damage by scavenging endogenous ROS. Like other antioxidant compounds, the ARW enables dilution of the effect of H_2O_2 on activating MAPK signaling. In addition, we also showed that catalase activity was stimulated in DLD1 upon H_2O_2 treatment but not in ARW groups. Stimulated levels of catalase upon H_2O_2 treatment were also observed in several cell lines and recovered by antioxidant treatment [36–38].

Furthermore, we evaluated the extent of H_2O_2-induced oxidative stress in the mitochondria and how ARW regulated this stress response. Oxidative phosphorylation in the mitochondria is the primary generator of intracellular ROS. Depending on the magnitude of oxidative stress, the ROS can be beneficial or damaging molecules in the cell. As a result, numerous mechanisms in the cell, including the antioxidant system and autophagy, meticulously keep ROS production under control [39]. Excessive ROS can compromise mitochondrial function in intestinal epithelia and overwhelm the cytoprotective pathways, resulting in apoptotic cell death and loss of the mucosal barrier [40]. We illustrated the mechanism of action of ARW in protecting mitochondria from oxidative damage. Several studies have shown H_2O_2-induced mitochondrial fragmentation on varieties of cell lines [41–45]. Similar to other studies, we found that oxidative stress enhanced mitochondrial fragmentation by increasing DRP1 phosphorylation (S616) which can be rescued by antioxidant treatment [46–49]. In addition, we found alterations in the L-OPA1 and S-OPA1 ratio in H_2O_2-induced DLD1 that are restored by ARW treatment. OPA1 is essential for the integrity of mitochondrial cristae, which house the electron transport chain complexes required to sustain the electrochemical gradient, as well as for the reduction of mitochondrial ROS levels [50]. Likewise, increased ROS levels cause shifts in mitochondrial membrane potential [51]. We also detected mitochondrial membrane-potential depolarization in DLD1 following H_2O_2 treatment, which ARW partially restored. Endogenous and exogenous antioxidants are known to maintain mitochondrial membrane potential during oxidative stress. These antioxidants inhibit rapid mitochondrial membrane polarization which is essential in the regulation of mitochondrial dynamics [52–55]. Taken together, ARW preserves mitochondrial structural integrity to reduce mitochondrial dysfunction during elevated oxidative stress.

Lastly, we investigated the impact of ARW in stressed intestinal epithelial cells and how it affects immunological function. Macrophages are distinguished by their plasticity and heterogeneity, and they are functionally reprogrammed into polarized phenotypes in response to various stimuli [56,57]. In view of this, we utilized murine macrophage Raw 264.7 cell lines to examine immunological cadence following exposure to culture supernatant of H_2O_2-induced DLD1. We postulated that oxidative stress in the gut induces intestinal epithelial cells to release inflammatory cytokines, which influence immunological responses in the host. As expected, we observed immunokine modulation in macrophages, with levels of IL6, IL10, MCP-1, TNF-α, and RANTES much higher in Raw 264.7 cells exposed to culture supernatant of H_2O_2-induced DLD1 compared to other groups. Excessive and unregulated production of chemokine/cytokines of macrophage and other immune cells can result in acute and chronic inflammatory disorders. Elevated levels of IL-6 and TNF-α in the gut would serve as prognostic markers as well as risk-stratification tools for evaluating intestinal inflammation and barrier failure [58]. Increased expression of the chemokines MCP-1 and RANTES are associated with Crohn's disease and ulcerative colitis [59–61]. These findings imply that oxidative stress in intestinal epithelial cells can potentially trigger local and systemic inflammation by transforming macrophages into an inflammatory phenotype. Overall, ARW suppresses macrophage production of inflammatory chemokines/cytokines via resolving intestinal barrier dysfunction.

Author Contributions: Conceptualization, S.-K.K. and J.M.A.; methodology, A.F., C.-S.K., Y.J.J. and J.M.A.; writing—original draft preparation, S.-K.K., J.M.A. and A.F.; writing—review and editing, S.-K.K., J.M.A. and A.F. All authors have read and agreed to the published version of the manuscript.

Institutional Review Board Statement: Not applicable.

Informed Consent Statement: Not applicable.

Data Availability Statement: The data presented in this study are available within the article (tables and figures).

Conflicts of Interest: The authors declare no conflict of interest.

References

1. Schoultz, I.; Keita, Å.V. The intestinal barrier and current techniques for the assessment of gut permeability. *Cells* **2020**, *9*, 1909. [CrossRef]
2. Cavin, J.-B.; Cuddihey, H.; MacNaughton, W.K.; Sharkey, K.A.J. Acute regulation of intestinal ion transport and permeability in response to luminal nutrients: The role of the enteric nervous system. *Am. J. Physiol. Gastrointest. Liver Physiol.* **2020**, *318*, G254–G264. [CrossRef]
3. Wang, Y.; Chen, Y.; Zhang, X.; Lu, Y.; Chen, H. New insights in intestinal oxidative stress damage and the health intervention effects of nutrients: A review. *J. Funct. Foods* **2020**, *75*, 104248. [CrossRef]
4. Chelakkot, C.; Ghim, J.; Ryu, S.H.J. Mechanisms regulating intestinal barrier integrity and its pathological implications. *Exp. Mol. Med.* **2018**, *50*, 1–9. [CrossRef]
5. Bhattacharyya, A.; Chattopadhyay, R.; Mitra, S.; Crowe, S.E.J. Oxidative stress: An essential factor in the pathogenesis of gastrointestinal mucosal diseases. *Physiol. Rev.* **2014**, *94*, 329–354. [CrossRef] [PubMed]
6. Thoo, L.; Noti, M.; Krebs, P. Keep calm: The intestinal barrier at the interface of peace and war. *Cell Death Dis.* **2019**, *10*, 849. [CrossRef] [PubMed]
7. Weidinger, A.; Kozlov, A.V. Biological activities of reactive oxygen and nitrogen species: Oxidative stress versus signal transduction. *Biomolecules* **2015**, *5*, 472–484. [CrossRef]
8. Zorov, D.B.; Juhaszova, M.; Sollott, S.J. Mitochondrial ros-induced ros release: An update and review. *Biochim. Biophys. Acta* **2006**, *1757*, 509–517. [CrossRef]
9. Sies, H.; Jones, D. Reactive oxygen species (ros) as pleiotropic physiological signalling agents. *Nat. Rev. Mol. Cell Biol.* **2020**, *21*, 363–383. [CrossRef] [PubMed]
10. Choi, H.D.; Kim, K.-Y.; Park, K.I.; Kim, S.-H.; Park, S.-G.; Yu, S.-N.; Kim, Y.-W.; Kim, D.S.; Chung, K.T.; Ahn, S.-C.J.M.; et al. Dual role of reactive oxygen species in autophagy and apoptosis induced by compound pn in prostate cancer cells. *Mol. Cell Toxicol.* **2021**, *17*, 41–50. [CrossRef]
11. Shields, H.J.; Traa, A.; Van Raamsdonk, J.M. Beneficial and detrimental effects of reactive oxygen species on lifespan: A comprehensive review of comparative and experimental studies. *Front. Cell Dev. Biol.* **2021**, *9*, 181. [CrossRef]

12. Ballway, J.W.; Song, B.-J.J. Translational approaches with antioxidant phytochemicals against alcohol-mediated oxidative stress, gut dysbiosis, intestinal barrier dysfunction and fatty liver disease. *Antioxidants* **2021**, *10*, 384. [CrossRef] [PubMed]

13. Deledda, A.; Annunziata, G.; Tenore, G.C.; Palmas, V.; Manzin, A.; Velluzzi, F.J. Diet-derived antioxidants and their role in inflammation, obesity and gut microbiota modulation. *Antioxidants* **2021**, *10*, 708. [CrossRef] [PubMed]

14. He, L.-X.; Wang, J.-B.; Sun, B.; Zhao, J.; Li, L.; Xu, T.; Li, H.; Sun, J.-Q.; Ren, J.; Liu, R.J. Suppression of tnf-α and free radicals reduces systematic inflammatory and metabolic disorders: Radioprotective effects of ginseng oligopeptides on intestinal barrier function and antioxidant defense. *J. Nutr. Biochem.* **2017**, *40*, 53–61. [CrossRef]

15. Hu, Q.; Ren, J.; Li, G.; Wu, J.; Wu, X.; Wang, G.; Gu, G.; Ren, H.; Hong, Z.; Li, J.J. The mitochondrially targeted antioxidant mitoq protects the intestinal barrier by ameliorating mitochondrial DNA damage via the nrf2/are signaling pathway. *Cell Death Dis.* **2018**, *9*, 403. [CrossRef] [PubMed]

16. Zhu, L.; Zhao, K.; Chen, X.; Xu, J. Impact of weaning and an antioxidant blend on intestinal barrier function and antioxidant status in pigs. *J. Anim. Sci.* **2012**, *90*, 2581–2589. [CrossRef]

17. Liu, W.-C.; Guo, Y.; Zhihui, Z.; Jha, R.; Balasubramanian, B. Algae-derived polysaccharides promote growth performance by improving antioxidant capacity and intestinal barrier function in broiler chickens. *Front. Vet. Sci.* **2020**, *7*, 990. [CrossRef]

18. Pandey, K.B.; Rizvi, S.I. Plant polyphenols as dietary antioxidants in human health and disease. *Oxid. Med. Cell. Longev.* **2009**, *2*, 270–278. [CrossRef]

19. Kumar Singh, A.; Cabral, C.; Kumar, R.; Ganguly, R.; Kumar Rana, H.; Gupta, A.; Rosaria Lauro, M.; Carbone, C.; Reis, F.; Pandey, A.K.J. Beneficial effects of dietary polyphenols on gut microbiota and strategies to improve delivery efficiency. *Nutrients* **2019**, *11*, 2216. [CrossRef]

20. Yang, E.-J.; Kim, J.-R.; Ryang, Y.-S.; Kim, D.-H.; Deung, Y.-K.; Park, S.-K.; Lee, K.-J. A clinical trial of orally administered alkaline reduced water. *Biomed. Sci. Lett.* **2007**, *13*, 83–89.

21. Ignacio, R.M.C.; Joo, K.-B.; Lee, K.-J.J. Clinical effect and mechanism of alkaline reduced water. *J. Food Drug Anal.* **2012**, *20*, 394–397. [CrossRef]

22. Jackson, K.; Dressler, N.; Ben-Shushan, R.S.; Meerson, A.; LeBaron, T.W.; Tamir, S.J. Effects of alkaline-electrolyzed and hydrogen-rich water, in a high-fat-diet nonalcoholic fatty liver disease mouse model. *World J. Gastroenterol.* **2018**, *24*, 5095. [CrossRef] [PubMed]

23. Lee, K.-J.; Park, S.-K.; Kim, J.-W.; Kim, G.-Y.; Ryang, Y.-S.; Kim, G.-H.; Cho, H.-C.; Kim, S.-K.; Kim, H.-W.J. Anticancer effect of alkaline reduced water (international conference on mind body science: Physical and physiological approach joint with the eighteenth symposium on life information science). *J. Int. Soc. Life Inf. Sci.* **2004**, *22*, 302–305.

24. Bertoni, M.; Oliveri, F.; Manghetti, M.; Boccolini, E.; Bellomini, M.G.; Blandizzi, C.; Bonino, F.; Del Tacca, M.J. Effects of a bicarbonate-alkaline mineral water on gastric functions and functional dyspepsia: A preclinical and clinical study. *Pharmacol. Res.* **2002**, *46*, 525–531. [CrossRef]

25. Koufman, J.A.; Johnston, N.J. Potential benefits of ph 8.8 alkaline drinking water as an adjunct in the treatment of reflux disease. *Ann. Otol. Rhinol. Laryngol.* **2012**, *121*, 431–434. [CrossRef] [PubMed]

26. Shin, D.W.; Yoon, H.; Kim, H.S.; Choi, Y.J.; Shin, C.M.; Park, Y.S.; Kim, N.; Lee, D.H. Effects of alkaline-reduced drinking water on irritable bowel syndrome with diarrhea: A randomized double-blind, placebo-controlled pilot study. *Evid.-Based Complement. Altern. Med.* **2018**, *2018*. [CrossRef] [PubMed]

27. Ungewiß, H.; Vielmuth, F.; Suzuki, S.T.; Maiser, A.; Harz, H.; Leonhardt, H.; Kugelmann, D.; Schlegel, N.; Waschke, J. Desmoglein 2 regulates the intestinal epithelial barrier via p38 mitogen-activated protein kinase. *Sci. Rep.* **2017**, *7*, 6329. [CrossRef]

28. Rias, Y.A.; Kurniawan, A.L.; Chang, C.W.; Gordon, C.J.; Tsai, H.T. Synergistic effects of regular walking and alkaline electrolyzed water on decreasing inflammation and oxidative stress, and increasing quality of life in individuals with type 2 diabetes: A community based randomized controlled trial. *Antioxidants* **2020**, *9*, 946. [CrossRef] [PubMed]

29. Lee, Y.-H.; Chang, J.-J.; Chien, C.-T.; Yang, M.-C.; Chien, H.-F.J. Antioxidant sol-gel improves cutaneous wound healing in streptozotocin-induced diabetic rats. *Exp. Diabetes Res.* **2012**, *2012*. [CrossRef]

30. Vergauwen, H.; Tambuyzer, B.; Jennes, K.; Degroote, J.; Wang, W.; De Smet, S.; Michiels, J.; Van Ginneken, C. Trolox and ascorbic acid reduce direct and indirect oxidative stress in the ipec-j2 cells, an in vitro model for the porcine gastrointestinal tract. *PLoS ONE* **2015**, *10*, e0120485. [CrossRef]

31. Hamasaki, T.; Harada, G.; Nakamichi, N.; Kabayama, S.; Teruya, K.; Fugetsu, B.; Gong, W.; Sakata, I.; Shirahata, S.J. Electro-chemically reduced water exerts superior reactive oxygen species scavenging activity in ht1080 cells than the equivalent level of hydrogen-dissolved water. *PLoS ONE* **2017**, *12*, e0171192. [CrossRef] [PubMed]

32. Park, W.H. The effect of mapk inhibitors and ros modulators on cell growth and death of h2o2-treated hela cells. *Mol. Med. Rep.* **2013**, *8*, 557–564. [CrossRef]

33. Rehfeldt, S.C.H.; Laufer, S.; Goettert, M.I. A highly selective in vitro jnk3 inhibitor, fmu200, restores mitochondrial membrane potential and reduces oxidative stress and apoptosis in sh-sy5y cells. *Int. J. Mol. Sci.* **2021**, *22*, 3701. [CrossRef]

34. Ren, H.; Meng, Q.; Yepuri, N.; Du, X.; Sarpong, J.O.; Cooney, R.N. Protective effects of glutathione on oxidative injury induced by hydrogen peroxide in intestinal epithelial cells. *J. Surg. Res.* **2018**, *222*, 39–47. [CrossRef] [PubMed]

35. Begum, R.; Kim, C.-S.; Fadriquela, A.; Bajgai, J.; Jing, X.; Kim, D.-H.; Kim, S.-K.; Lee, K.-J. Molecular hydrogen protects against oxidative stress-induced raw 264.7 macrophage cells through the activation of nrf2 and inhibition of mapk signaling pathway. *Mol. Cell Toxicol.* **2020**, *16*, 103–118. [CrossRef]

36. Konyalioglu, S.; Armagan, G.; Yalcin, A.; Atalayin, C.; Dagci, T.J. Effects of resveratrol on hydrogen peroxide-induced oxidative stress in embryonic neural stem cells. *Neural Regen. Res.* **2013**, *8*, 485.

37. Mirzaei, M.; Mirdamadi, S.; Safavi, M.; Zare, D.; Hadizadeh, M.; Asadi, M.M. Synthesis, in vitro and cellular antioxidant activity evaluation of novel peptides derived from saccharomyces cerevisiae protein hydrolysate: Structure–function relationship. *Amino Acids* **2019**, *51*, 1167–1175. [CrossRef]

38. Park, W.H. Anti-apoptotic effect of caspase inhibitors on h2o2-treated hela cells through early suppression of its oxidative stress. *Oncol. Rep.* **2014**, *31*, 2413–2421. [CrossRef]

39. Kaminskyy, V.O.; Zhivotovsky, B.J. Free radicals in cross talk between autophagy and apoptosis. *Antioxid. Redox Signal.* **2014**, *21*, 86–102. [CrossRef] [PubMed]

40. Aviello, G.; Knaus, U.J. Ros in gastrointestinal inflammation: Rescue or sabotage? *Br. J. Pharmacol.* **2017**, *174*, 1704–1718. [CrossRef]

41. Debattisti, V.; Gerencser, A.A.; Saotome, M.; Das, S.; Hajnóczky, G.J. Ros control mitochondrial motility through p38 and the motor adaptor miro/trak. *Cell Rep.* **2017**, *21*, 1667–1680. [CrossRef] [PubMed]

42. Fan, X.; Hussien, R.; Brooks, G.A.J. H2o2-induced mitochondrial fragmentation in c2c12 myocytes. *Free Radic. Biol. Med.* **2010**, *49*, 1646–1654. [CrossRef]

43. Su, Y.C.; Chiu, H.W.; Hung, J.C.; Hong, J.R. Beta-nodavirus b2 protein induces hydrogen peroxide production, leading to drp1-recruited mitochondrial fragmentation and cell death via mitochondrial targeting. *Apoptosis* **2014**, *19*, 1457–1470. [CrossRef]

44. Wang, J.; Aung, L.H.; Prabhakar, B.S.; Li, P. The mitochondrial ubiquitin ligase plays an anti-apoptotic role in cardiomyocytes by regulating mitochondrial fission. *J. Cell. Mol. Med.* **2016**, *20*, 2278–2288. [CrossRef] [PubMed]

45. Willems, P.H.; Rossignol, R.; Dieteren, C.E.; Murphy, M.P.; Koopman, W.J. Redox homeostasis and mitochondrial dynamics. *Cell Metab.* **2015**, *22*, 207–218. [CrossRef] [PubMed]

46. Gan, X.; Huang, S.; Yu, Q.; Yu, H.; Yan, S.S.J. Blockade of drp1 rescues oxidative stress-induced osteoblast dysfunction. *Biochem. Biophys. Res. Commun.* **2015**, *468*, 719–725. [CrossRef]

47. Kim, M.H.; Kwon, S.Y.; Woo, S.-Y.; Seo, W.D.; Kim, D.Y.J. Antioxidative effects of chrysoeriol via activation of the nrf2 signaling pathway and modulation of mitochondrial function. *Molecules* **2021**, *26*, 313. [CrossRef]

48. Li, C.-J.; Sun, L.-Y.; Pang, C.-Y.J. Synergistic protection of n-acetylcysteine and ascorbic acid 2-phosphate on human mesenchymal stem cells against mitoptosis, necroptosis and apoptosis. *Sci. Rep.* **2015**, *5*, 9819. [CrossRef]

49. Watanabe, T.; Saotome, M.; Nobuhara, M.; Sakamoto, A.; Urushida, T.; Katoh, H.; Satoh, H.; Funaki, M.; Hayashi, H. Roles of mitochondrial fragmentation and reactive oxygen species in mitochondrial dysfunction and myocardial insulin resistance. *Exp. Cell Res.* **2014**, *323*, 314–325. [CrossRef]

50. Quintana-Cabrera, R.; Manjarrés-Raza, I.; Vicente-Gutiérrez, C.; Corrado, M.; Bolaños, J.P.; Scorrano, L. Opa1 relies on cristae preservation and atp synthase to curtail reactive oxygen species accumulation in mitochondria. *Redox Biol.* **2021**, *41*, 101944. [CrossRef] [PubMed]

51. Zhang, X.; Lee, M.D.; Wilson, C.; McCarron, J.G. Hydrogen peroxide depolarizes mitochondria and inhibits ip3-evoked Ca^{2+} release in the endothelium of intact arteries. *Cell Calcium* **2019**, *84*, 102108. [CrossRef]

52. Cossu, A.; Posadino, A.M.; Giordo, R.; Emanueli, C.; Sanguinetti, A.M.; Piscopo, A.; Poiana, M.; Capobianco, G.; Piga, A.; Pintus, G.J. Apricot melanoidins prevent oxidative endothelial cell death by counteracting mitochondrial oxidation and membrane depolarization. *PLoS ONE* **2012**, *7*, e48817. [CrossRef]

53. Distelmaier, F.; Visch, H.-J.; Smeitink, J.A.; Mayatepek, E.; Koopman, W.J.; Willems, P.H.J. The antioxidant trolox restores mitochondrial membrane potential and Ca^{2+}-stimulated atp production in human complex i deficiency. *J. Mol. Med.* **2009**, *87*, 515–522. [CrossRef]

54. Marquez, J.; Park, N.; Garcia, M.V.F.; Kim, H.K.; Han, J.J. Hs-1793 protects c2c12 cells from oxidative stress via mitochondrial function regulation. *Mol. Cell Toxicol.* **2020**, *16*, 359–365. [CrossRef]

55. Park, C.; Lee, H.; Park, S.-H.; Hong, S.H.; Song, K.S.; Cha, H.-J.; Kim, G.-Y.; Chang, Y.-C.; Kim, S.; Kim, H.-S.; et al. Indole-6-carboxaldehyde prevents oxidative stress-induced mitochondrial dysfunction, DNA damage and apoptosis in c2c12 skeletal myoblasts by regulating the ros-ampk signaling pathway. *Mol. Cell Toxicol.* **2020**, *16*, 455–467. [CrossRef]

56. Kalathil, S.G.; Thanavala, Y.J. High immunosuppressive burden in cancer patients: A major hurdle for cancer immunotherapy. *Cancer Immunol. Immunother.* **2016**, *65*, 813–819. [CrossRef] [PubMed]

57. Liu, C.-P.; Zhang, X.; Tan, Q.-L.; Xu, W.-X.; Zhou, C.-Y.; Luo, M.; Li, X.; Huang, R.-Y.; Zeng, X.J. Nf-κb pathways are involved in m1 polarization of raw 264.7 macrophage by polyporus polysaccharide in the tumor microenvironment. *PLoS ONE* **2017**, *12*, e0188317. [CrossRef]

58. Xiao, Y.-T.; Yan, W.-H.; Cao, Y.; Yan, J.-K.; Cai, W. Neutralization of il-6 and tnf-α ameliorates intestinal permeability in dss-induced colitis. *Cytokine* **2016**, *83*, 189–192. [CrossRef] [PubMed]

59. Ajuebor, M.N.; Das, A.M.; Virág, L.; Flower, R.J.; Szabó, C.; Perretti, M.J. Role of resident peritoneal macrophages and mast cells in chemokine production and neutrophil migration in acute inflammation: Evidence for an inhibitory loop involving endogenous il-10. *J. Immunol.* **1999**, *162*, 1685–1691.

60. Ajuebor, M.N.; Swain, M.G.J. Role of chemokines and chemokine receptors in the gastrointestinal tract. *Immunology* **2002**, *105*, 137–143. [CrossRef]

61. Cassatella, M.A.J. The production of cytokines by polymorphonuclear neutrophils. *Immunolol. Today* **1995**, *16*, 21–26. [CrossRef]